Article

Large-Gap Quantum Spin Hall Insulators in Two-Dimensional Hafnium Halides: Unraveling the Impact of Strain and Substrate

Ruishen Meng,* Lino M. C. Pereira, Joris Van de Vondel, Jin Won Seo, Jean-Pierre Locquet, and Michel Houssa*

Read Online

ACCESS | Metrics & More | Article Recommendations | Supporting Information

ABSTRACT: Two-dimensional (2D) topological insulators (TIs) or quantum spin Hall (QSH) insulators, characterized by insulating 2D electronic band structures and metallic helical edge states protected by time-reversal symmetry, offer a platform for realizing the quantum spin Hall effect, making them promising candidates for future spintronic devices and quantum computing. However, observing a high-temperature quantum spin Hall effect requires large-gap 2D TIs, and only a few 2D systems have been experimentally confirmed to possess this property. In this study, we employ first-principles calculations, combined with a structural search based on an evolutionary algorithm, to predict a class of 2D QSH insulators in hafnium halides, namely, HfF, HfCl, and HfBr with sizable band gaps of 0.12, 0.19, and 0.38 eV. Their topological nontrivial nature is confirmed by a Z_2 invariant which equals to 1 and the presence of gapless edge states. Furthermore, the QSH effect in these materials remains robust under biaxial tensile strain of up to 10%, and the use of h-BN as a substrate effectively preserves the QSH states in these materials. Our findings pave the way for future theoretical and experimental investigations of 2D hafnium halides and their potential for realizing the QSH effect.
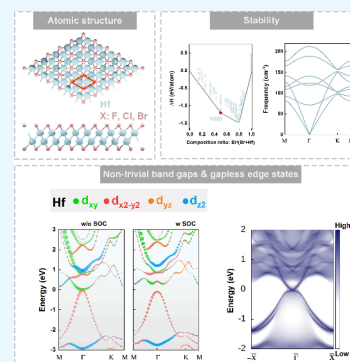
INTRODUCTION

Topological insulators (TIs) have garnered significant research interest in condensed matter physics and materials science due to their unique properties, namely, the presence of gapless Dirac cone-like edge/surface states within the bulk electronic band gaps, which are topologically protected from backscattering by time-reversal symmetry.[1,2] The edge states in two-dimensional (2D) TIs, also known as quantum spin Hall (QSH) insulators, exhibit greater resilience against elastic backscattering and localization compared to the surface states of three-dimensional TIs.[3] This enhanced robustness makes the edge states of 2D TIs highly promising for achieving dissipationless electron transport, thus offering great potential for the development of low-power and multifunctional spintronic devices.

In the broader landscape of 2D materials, a variety of monolayers have emerged with distinct structural, electronic, and magnetic properties that hold their own potential in various applications.[4−6] The exploration of these materials, alongside TIs, enriches our understanding of 2D material systems and their diverse functionalities.

The concept of the QSH effect was initially proposed in graphene, serving as a foundational model for studying this intriguing phenomenon.[7] Subsequentially, other 2D TIs based on group IV and V elements, i.e., silicene, germanene, stanene, arsenene, antimonene, and their functionalized counterparts, were also theoretically predicted.[3,8−15] In addition, many other 2D compounds were also predicted to be 2D TIs, such as the

1T′ phase of transition-metal dichalcogenides,[16] oxygen-functionalized group III monochalcogenides,[17] Mxene,[18] SiTe,[19] ZrTe$_5$, HfTe$_5$,[20] Bi$_4$Br$_4$,[21] etc. However, the experimental verification of the quantum spin Hall (QSH) effect in 2D materials has been quite challenging. It was only first achieved in HgTe/CdTe quantum wells at a temperature of approximately 10 K.[22] To date, the monolayer of 1T′-WTe$_2$ stands as the sole 2D crystal that has been experimentally confirmed to host QSH states. But even for this material, the observation was limited to a relatively low temperature of 100 K.[23] The small bulk band gaps and the difficulty in synthesizing high-quality 2D crystals as well as realizing their chemical functionalization could be the primary obstacles hindering the experimental verification of more 2D TIs at higher temperatures.[24,25] Therefore, it is of paramount importance to continue the theoretical exploration for 2D TIs with high stability and large nontrivial band gaps.[26−29]

2D zirconium and hafnium halides, identified as a promising family of quantum spin Hall insulators with substantial nontrivial band gaps,[30] hold great potential for experimental exploration of the QSH effect at more accessible and practical
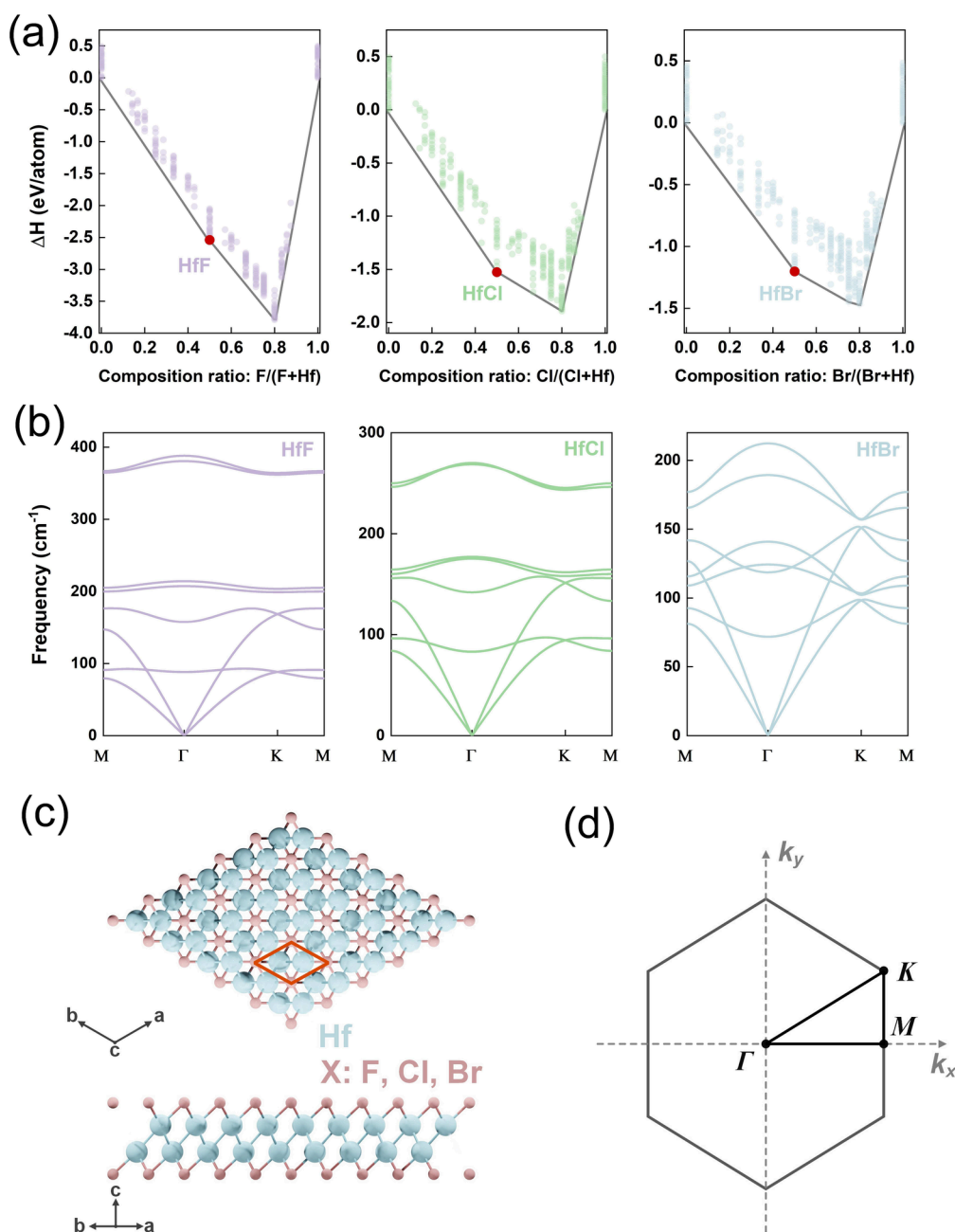
Figure 1. (a) Convex hulls of different stoichiometries searched by USPEX; (b) phonon dispersion spectra; (c) top and side views of the atomic structure of 2D HfF, HfCl, and HfBr; and (d) the first Brillouin zone.

temperatures. In this study, we conducted a comprehensive structural search for potential atomic configurations of 2D hafnium halides through a combination of first-principles calculations and an evolutionary algorithm method. Our investigations reveal that 2D hafnium monohalides (HfX, where X = F, Cl, Br) exhibit high energetic, dynamic, and thermal stabilities. Utilizing hybrid functional calculations, we confirm all three monolayers as 2D topological TIs with sizable nontrivial bulk gaps. Furthermore, we delve into the impact of strain on 2D HfBr, discovering that the band gap is highly responsive to biaxial compressive strain, disappearing when the compressive strain exceeds 2%. Furthermore, the band gap, along with the QSH states, proves less sensitive to biaxial tensile strain, even up to 10%. Additionally, our findings suggest that h-BN serves as an ideal substrate for preserving the

QSH states of 2D HfBr, offering encouraging prospects for practical applications.

■ RESULTS

The global search for all possible 2D atomic structures of hafnium halides was performed using the Universal Structure Predictor: Evolutionary Xtallography (USPEX) method based on an evolutionary algorithm. The resulting convex hulls, representing the relationship between the enthalpy of formation and the composition of the 2D hafnium halides with various stoichiometries, are depicted in Figure 1(a). The convex hull plots clearly show the energetic stability of HfX, HfX_4, and/or HfX_3 (in the case of $HfBr_3$) based on their formation enthalpies. It is noteworthy that while the formation enthalpies of HfX_4/HfX_3 are positioned on the convex hulls,
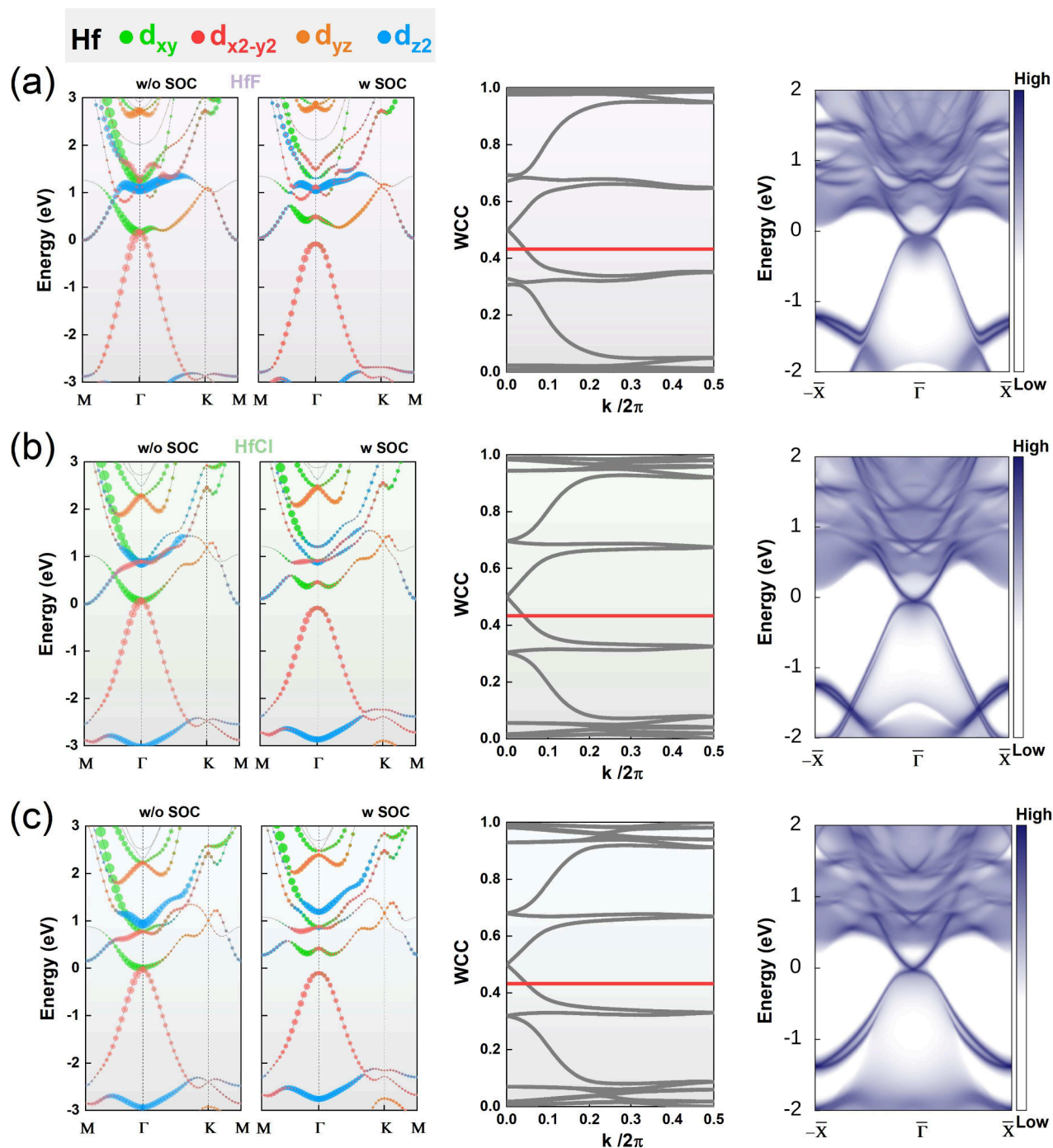
Figure 2. Orbital-projected band structures without and with SOC, evolution of Wannier charge centers (WCCs) in the Brillouin zone, and the topological edge states along the zigzag direction of 2D (a) HfF, (b) HfCl, and (c) HfBr. The Fermi level is set to zero.

their atomic structures may not exclusively be 2D and could also be one-dimensional. Additional details regarding their atomic structures can be found in Figure S1 in the Supporting Information. Concerning HfF, HfCl, and HfBr, their atomic configurations all exist within a 2D framework, as depicted in Figure 1(d). With the expectation of observing analogous electronic properties across these configurations, we direct our attention to this particular 2D HfX phase. However, it is worth mentioning that other stoichiometries may also hold promise for future research endeavors. The unit cell of the 2D HfX structure consists of four atoms, comprising two Hf atoms and two halogen atoms. These atoms are arranged in a stacked

configuration, with the sequence X-Hf-Hf-X along the out-of-plane direction. Within the structure, each X atom forms bonds with three neighboring Hf atoms, while each Hf atom exhibits 6-fold coordination, being bonded to three X atoms and three Hf atoms, respectively. The 2D HfX structures exhibit trigonal symmetry, characterized by a space group of $P3m1$ and a point group of D_{3d}. The in-plane lattice constants of 2D HfF, HfCl and HfBr are calculated to be 3.22, 3.39, and 3.49 Å, respectively, and their Hf−Hf (Hf−X) bond lengths are 2.28 (2.97), 2.63 (3.01), and 2.77 (3.02) Å, respectively.

Phonon dispersion calculations, in conjunction with ab initio molecular dynamics (AIMD) simulations, were conducted to
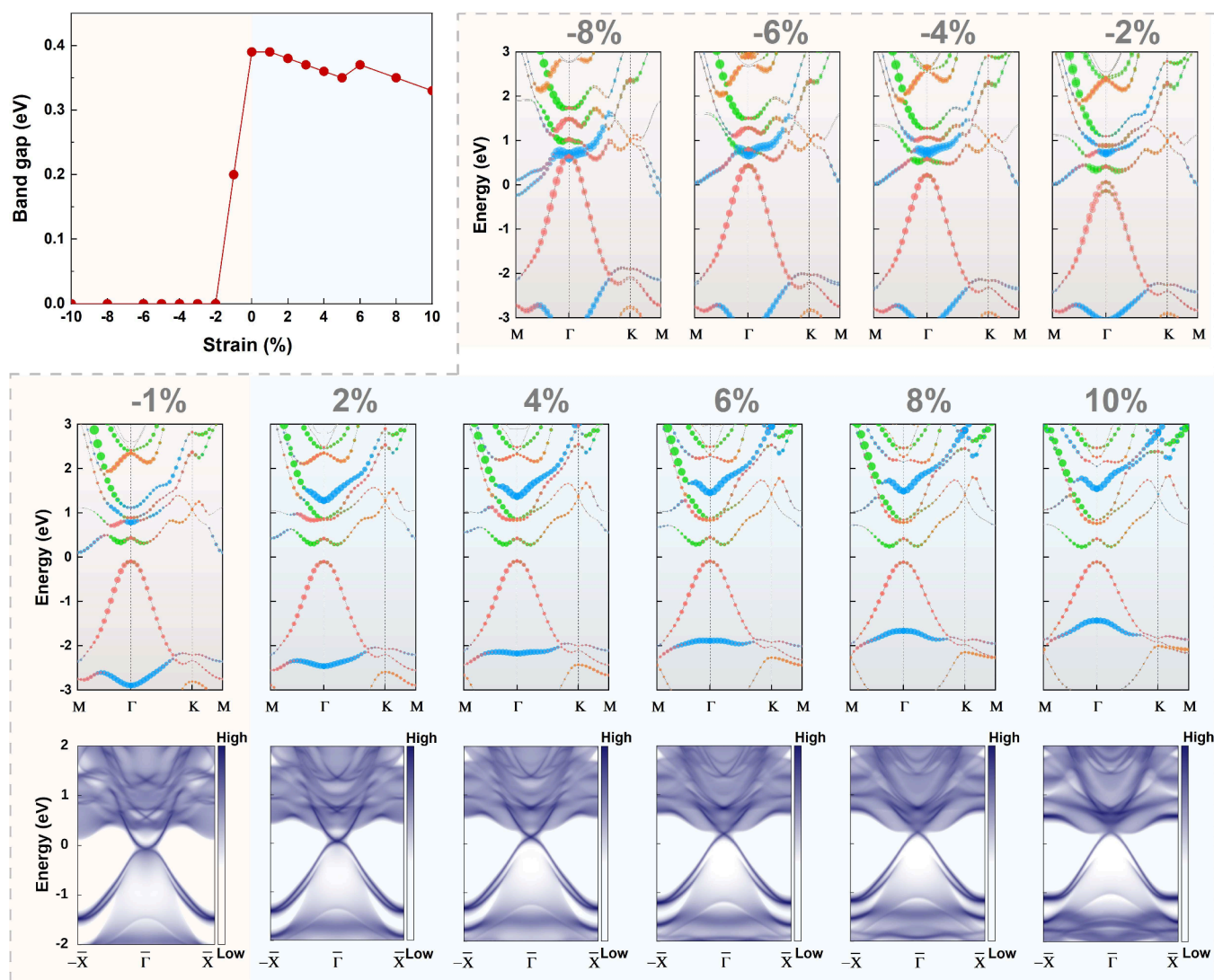
Figure 3. Variations of bulk band gap under biaxial strain for 2D HfBr and the corresponding orbital-decomposed band structures and the topological edge states along the zigzag direction for 2D HfBr. The Fermi level is set to zero.

assess both the dynamic and thermal stability of the 2D HfX structures. The results are depicted in Figure 1(b) and Figure S2, respectively. The phonon dispersion spectra reveal the absence of any imaginary modes, indicating the dynamic stability of all three 2D materials. Furthermore, during the AIMD simulations at a fixed temperature of 600 K, the energies of the 2D materials exhibit minimal fluctuations within narrow ranges of approximately 5 eV/cell. Additionally, the square root of the mean squared displacement (sqrt-(MSD)) is found to be smaller than 0.3 Å, indicating that the atoms experience only slight oscillations around their equilibrium positions. This observation is further corroborated by the atomic structure variation at different simulation times (Figure S2(b)). Hence, it can be inferred that these materials possess high thermal stability.

To facilitate potential experimental preparation and identification, we computed the phase diagram for 2D HfBr using the method outlined in refs 31 and 32 by calculating the grand potential associated with each crystal structure. Additionally, Raman spectra were computed by density functional perturbation theory (DFPT) for the three 2D HfX materials, and these are presented in Figures S3 and S4, respectively. In

the phase diagram, considering realistic Br_2 pressures ranging from approximately 10^{-12} to 10^{-2} atm, the growth temperature for 2D HfBr spans from ∼1100 to ∼2000 K. Taking 2D HfBr as a representative example for Raman spectrum analysis, the material reveals three distinctive peaks at frequencies of 68 cm^{-1} (in-plane mode), 128 cm^{-1} (in-plane mode), and 182 cm^{-1} (out-of-plane mode). Furthermore, a shoulder peak in the intermediate frequency range around 113 cm^{-1} can be attributed to an in-plane mode.

The electronic properties of the 2D HfX materials were explored by conducting orbital-decomposed band structure calculations using HSE06 exchange-correlation functionals, both with and without considering spin−orbit coupling (SOC) interactions. The results are depicted in the left panels of Figure 2. In the absence of SOC, the valence band maximum (VBM) and conduction band minimum (CBM) touch at the Γ point, which are primarily composed of the $d_{x^2-y^2}$ and d_{xy} orbitals of the Hf atoms, respectively. However, upon enabling SOC, band inversion takes place around the Γ point, forming a camelback-like band structure and resulting in band gap openings of 0.12, 0.19, and 0.38 eV for HfF, HfCl, and HfBr, respectively. This band inversion and the shape of the resulting
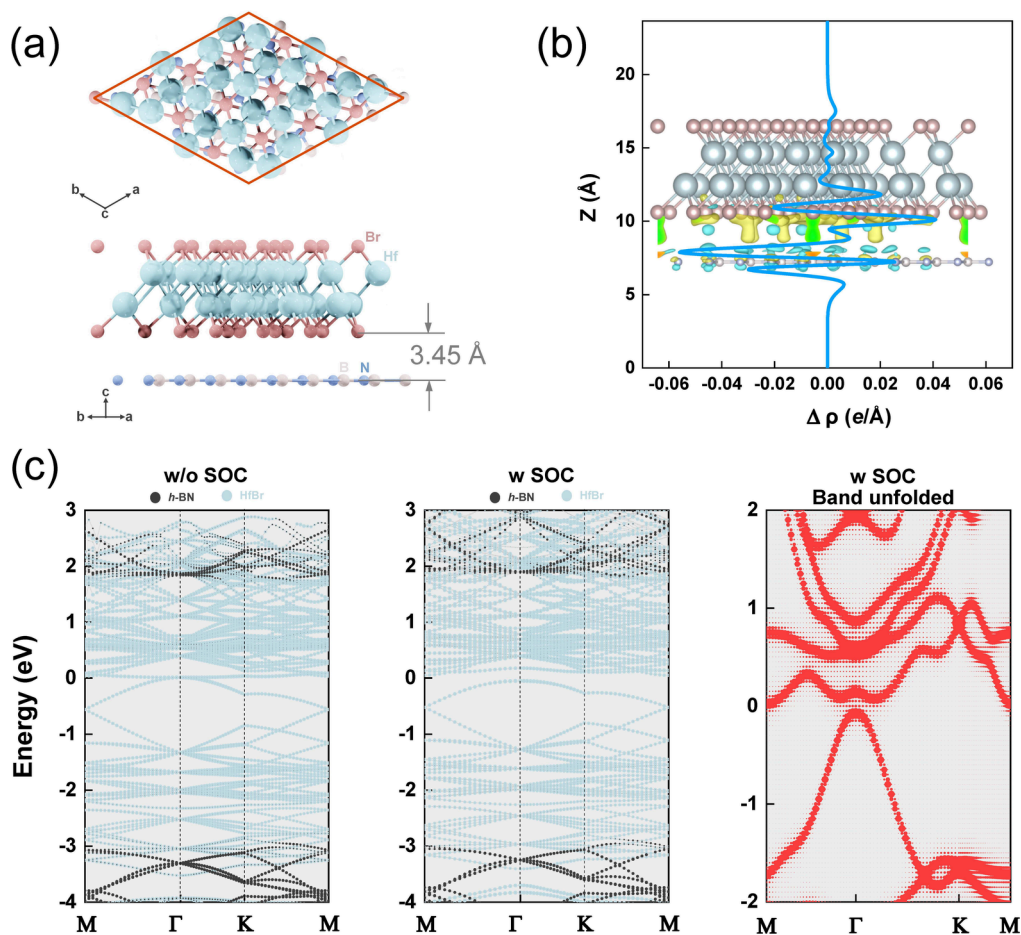
Figure 4. (a) Top and side views of the atomic structure. (b) Plane-averaged charge density difference $\Delta\rho$ (blue line) along the normal direction. The inset shows the 3D isosurface of the charge density difference, where the yellow and cyan areas represent electron accumulation and depletion, respectively. (c) Orbital-projected band structures without and with SOC, along with the unfolded band structure of the HfBr/h-BN heterobilayer. The Fermi level is set to zero.

band structure indicate the presence of nontrivial topology in these materials. Additionally, the band gap values of the 2D HfX materials are much larger than that of 1T′-WTe$_2$ (0.05 eV),[33] greatly surpassing the thermal broadening at room temperature. This suggests a favorable condition for the potential experimental observation of the topological states at elevated temperatures in these materials.

The topological properties of the 2D HfX were determined by calculating their Z_2 invariants using the vasp2trace program.[34] This method utilizes a set of elementary band representations (EBRs) to analyze whether the energy bands can be represented as linear combinations of these elementary representations. The results indicate that all three materials are TIs with a Z_2 number of 1.

To provide additional evidence for the topological character of the 2D HfX materials, their Z_2 topological invariants were further verified based on the evolution of the Wannier charge centers (WCCs) in reciprocal space,[35] as depicted in the middle panels of Figure 2. Notably, the Z_2 value was found to be equal to 1, as evidenced by the evolution of the WCCs along the Brillouin zone, which intersects a reference line (in red in the figure) with an odd number of points. This confirms that the 2D HfX materials are indeed nontrivial topological insulators.

To highlight the presence of topologically nontrivial edge states, we performed additional calculations to reveal the surface band structures, as presented in the right panels of Figure 2. It is evident that an odd number (one) of pairs of helical edge states traverse the bulk band gap, and these states are effectively protected from backscattering by the time-reversal symmetry. This unique protection mechanism enables dissipationless transport within these 2D halides.

In addition to 2D HfF, HfCl, and HfBr, we also explored the topological properties of 2D HfI. Its stability was verified through the absence of imaginary frequencies in the phonon dispersion spectrum, as well as the AIMD simulation, as depicted in Figure S5. Similar to the other three materials, the band inversion was observed in the band structure of 2D HfI with SOC, and its Z_2 number was found to be 1 using the vasp2trace program. However, in the WCC analysis, gaps were observed, potentially leading to a Z_2 value of 0, despite the large spreads of the Wannier functions of the Hf atom which is approximately 4 Å. Nevertheless, in the surface band structure, we observed two edge states connecting the VBM and the CBM in the bulk band structure. Consequently, 2D HfI exhibits strong indications of being a 2D topological insulator. Further confirmation is necessary to fully validate its topological properties.

Considering that HfBr possesses the largest nontrivial band gap among the studied materials, our subsequent investigation focuses on the impact of strain and substrate on this specific 2D material.

Figure 3 presents the band gap variation of 2D HfBr as a function of biaxial strain, along with the orbital-decomposed band structures and/or the corresponding surface band structures under different strain conditions. Here, negative and positive strain values denote compression and elongation, respectively. Under negative strain, the band gap shows a monotonous decrease, eventually vanishing at a strain of −2%. Conversely, the band gap exhibits less sensitivity to positive strain. Initially, it slightly decreases from 0.39 to 0.35 eV as the strain increases from 0 to 5%. Then, it experiences a slight increase to 0.37 eV at 6%, followed by a gradual decrease to 0.33 eV at 10%.

The variation in band gap is primarily attributed to the shifting of the Hf-d_{z^2} as well as the $d_{x^2-y^2}$ orbitals. Under negative strain, the Hf-d_{z^2} orbital at the M point of the first Brillouin zone shifts downward toward the Fermi level while the $d_{x^2-y^2}$ orbital at the Γ point shifts upward, resulting in a decrease in the band gap. Conversely, under positive strain, the Hf-d_{z^2} orbital shifts upward while the $d_{x^2-y^2}$ orbital and the camelback-like band shape and band inversion around the Γ point are barely affected. The WCCs of the 2D HfBr under strain are provided in Figure S6. The results reveal a Z_2 number of 1 across the strain range from −1 to 10%. Furthermore, the surface band structures reveal the presence of topologically protected conducting edge states, which bridge the bulk valence and conduction bands. These findings confirm that the QSH state in 2D HfBr is robust against tensile strain.

It has been demonstrated that the preservation of QSH states in 2D TIs critically relies on finding a suitable substrate, allowing for the experimental observation of the QSH effect.[36,37] Herein, we propose the h-BN monolayer as a promising candidate due to its wide application as a dielectric material in 2D electronics and its potential for cost-effective, high-quality synthesis.

After full relaxation, the lattice parameter of the h-BN monolayer was determined to be 2.51 Å, which is in good agreement with experiment. To mitigate the influence of lattice mismatch, we constructed HfBr/h-BN heterobilayers using a $\sqrt{13} \times \sqrt{13}$ HfBr supercell and a 5×5 h-BN supercell that contains a total of 102 atoms. As a result, the lattice mismatch was minimized to less than 0.2%. The relaxed atomic structure, charge density difference, and electronic properties of the HfBr/h-BN heterobilayers are illustrated in Figure 4. To account for the long-range van der Waals (vdW) interactions, the calculations were performed using the PBE-D3 method. The interlayer distance, measured between the h-BN plane and the lower Br atoms, was determined to be 3.45 Å, suggesting weak interlayer interactions in the heterobilayers.

To evaluate the structural stability of the heterobilayer, the binding energies were calculated by the following formula using the PBE-D3 method

$$E_b = E_{HfBr/h\text{-}BN} - E_{HfBr} - E_{h\text{-}BN}$$

where E_b represents the binding energy, $E_{HfBr/h\text{-}BN}$ is the total energy of the HfBr/h-BN heterobilayer, E_{HfBr} corresponds to the total energy of the $\sqrt{13} \times \sqrt{13}$ HfBr supercell, and $E_{h\text{-}BN}$ represents the total energy of the 5×5 h-BN supercell. The calculated binding energy was found to be approximately −16 meV/Å^2, closely aligning with the typical van der Waals binding energy of around −20 meV/Å^2 estimated by DFT calculations.[38] This result indicates a vdW interaction between the HfBr and h-BN layers.

To investigate the charge distribution in the heterobilayers, we examined the charge-density difference, denoted as $\Delta\rho = \rho_{HfBr/h\text{-}BN} - \rho_{HfBr} - \rho_{h\text{-}BN}$, as depicted in Figure 4(b). Here, $\rho_{HfBr/h\text{-}BN}$ represents the total charge density of the heterobilayers, and ρ_{HfBr} and $\rho_{h\text{-}BN}$ are the charge densities of the isolated HfBr and h-BN monolayers, respectively, at the same position within the heterostructure. The charge-density difference clearly reveals a redistribution of charge density at the interface of the heterobilayer, giving rise to electron-rich and hole-rich regions. This phenomenon suggests that charge accumulation occurs at the surfaces of h-BN while charge depletion takes place in the HfBr region. Notably, the Bader charge analysis indicates a total charge transfer of 0.002e, further suggesting a weak interlayer interaction between the two layers.

From the projected band structures of the heterobilayer in Figure 4(c), we observe that h-BN has a band gap of approximately 4.6 eV, which is consistent with previous DFT studies.[39] Without considering SOC, the conduction and valence bands of HfBr are degenerate at the Γ point and the Fermi level. However, upon introducing SOC, the degeneracy of the energy bands is lifted, leading to a band gap opening of 99 meV. This value is very close to the band gap of 82 meV obtained for the free-standing 2D HfBr using the PBE functional. To facilitate a comprehensive comparison between the band structures of the heterobilayer and the free-standing HfBr layer, the KPROJ program[40] was employed to obtain the unfolded bands of the heterobilayer with SOC. Remarkably, the shape of the unfolded bands around the Γ point near the Fermi level closely resembles those of the free-standing 2D HfBr. These results strongly suggest the preservation of band inversion and, consequently, the existence of quantum spin Hall states in 2D HfBr when utilizing the h-BN monolayer as a substrate.

■ CONCLUSIONS

We have performed comprehensive first-principles calculations to explore the structural, electronic, and topological properties of 2D hafnium halides. Our results demonstrate that these materials are promising 2D TIs with sizable band gaps of up to 0.38 eV. The stability of these structures was confirmed through phonon dispersion calculations and ab initio molecular dynamics simulations, indicating their suitability for practical applications. We have identified their topological nature using Z_2 invariants and revealed the existence of helical edge states, which are crucial for dissipationless transport and the QSH effect.

Additionally, we investigated the response of 2D HfBr to biaxial strain and found that the QSH state remains robust under tensile strain. Furthermore, we propose the h-BN monolayer as an ideal substrate, providing a favorable environment to preserve the QSH states of 2D HfBr. These findings highlight the potential of 2D hafnium halides as promising materials for future spintronic devices and quantum computing applications, owing to their remarkable electronic and topological properties.

■ METHODS

In this study, density functional theory (DFT) calculations were carried out using the Vienna ab initio simulation package (VASP),[41,42] employing projector augmented wave (PAW) pseudopotentials to describe the electron–ion interaction. The

generalized gradient approximation (GGA), parametrized by the Perdew−Burke−Ernzerhof (PBE) approach,[43] was used as the exchange correlation functional. The energy cutoff of 480 eV and k-point meshes of $0.03 \times 2\pi$ and $0.02 \times 2\pi$ Å^{-1} were used for structural optimizations and self-consistent calculations. A total energy convergence criterion of 10^{-6} eV/cell and a force convergence criterion of 0.001 eV/Å were chosen for complete relaxations of lattice constants as well as atomic positions. For a more accurate estimation of the band gap and band order, the HSE06 hybrid functional[44] with 25% of the exact exchange was used. Spin−orbit coupling (SOC) is included in electronic structure calculations. To prevent interaction between periodic images, a vacuum space larger than 15 Å was introduced along the z direction. Grimme's DFT-D3 method[45] was utilized to account for van der Waals (vdW) interactions in the heterobilayer calculations. Part of the postprocessing of the VASP-calculated data was conducted using the VASPKIT code.[46]

The search for potential 2D structures of hafnium halides was carried out using an ab initio evolutionary algorithm implemented in USPEX,[47] in combination with the VASP code. The exploration involved variable-composition searching, with the total number of atoms constrained within the range of 2 to 8 for the 2D crystals. To initiate the search, a set of 150 symmetry groups was utilized to generate random symmetric structures as the initial population. Subsequently, full structure relaxations were performed, and the most stable and metastable atomic structures were screened and carried forward into the next generation based on their formation enthalpy. The number of generations was set to 40. Structures with formation energies located on the convex hulls were identified as the most stable, while those with formation energies above the convex hulls were considered to be metastable structures.

Phonon dispersion curves were computed using the PHONOPY package[48] based on density functional perturbation theory (DFPT). For ab initio molecular dynamics (AIMD) simulations, $5 \times 5 \times 1$ supercells (with 100 atoms) were employed and equilibrated at 600 K for 300 ps with a time step of 1 fs. The AIMD simulations utilized a machine-learning-based force field[48] and employed the constant-temperature and -volume canonical ensemble (NVT) with temperature control achieved through a Nose thermostat.[49,50]

The maximally localized Wannier functions (MLWFs) using d orbitals of Hf and p orbitals of the halogen atoms as the initial projections are constructed using the WANNIER90 code.[51] From the MLWFs tight-binding Hamiltonian obtained, the topological invariants Z_2 number and the edge state are computed using the WannierTools package.[52] Specifically, the edge state is calculated using the iterative surface Green's function methods for a semi-infinite system.[53]

ASSOCIATED CONTENT

Data Availability Statement

The data sets used and/or analyzed during the current study are available from the corresponding author on reasonable request.

S Supporting Information

The Supporting Information is available free of charge at https://pubs.acs.org/doi/10.1021/acsomega.4c03502.

Top and side views of the atomic structures besides 2D HfX; Sqrt(MSD) and energy evolution at 600 K during AIMD simulations and the corresponding atomic structures at 50, 150, 250, and 300 ps for 2D HfBr, HfCl and HfF; calculated P−T phase diagram of the hafnium bromides identified through the USPEX structural search; simulated Raman spectra of 2D HfF, HfCl, and HfBr; stability and electronic and topological properties of 2D HfI; and evolution of WCCs in the Brillouin zone under biaxial strain from −1 to 10% for 2D HfBr (PDF)

AUTHOR INFORMATION

Corresponding Authors

Ruishen Meng − KU Leuven, Department of Physics and Astronomy, Semiconductor Physics Laboratory, Leuven B-3001, Belgium; orcid.org/0000-0002-6882-5768; Email: ruishen.meng@kuleuven.be

Michel Houssa − KU Leuven, Department of Physics and Astronomy, Semiconductor Physics Laboratory, Leuven B-3001, Belgium; imec, Leuven B-3001, Belgium; Email: michel.houssa@kuleuven.be

Authors

Lino M. C. Pereira − KU Leuven, Department of Physics and Astronomy, Quantum Solid-State Physics, Leuven B-3001, Belgium

Joris Van de Vondel − KU Leuven, Department of Physics and Astronomy, Quantum Solid-State Physics, Leuven B-3001, Belgium; orcid.org/0000-0001-6894-7258

Jin Won Seo − KU Leuven, Department of Materials Engineering, Leuven B-3001, Belgium; orcid.org/0000-0003-4937-0769

Jean-Pierre Locquet − KU Leuven, Department of Physics and Astronomy, Semiconductor Physics Laboratory, Leuven B-3001, Belgium

Complete contact information is available at:
https://pubs.acs.org/10.1021/acsomega.4c03502

Author Contributions

R.M. and M.H. conceptualized the work. R.M. was responsible for all of the calculations. The manuscript was written by R.M. and M.H. All authors contributed to the discussions and analyses of the data and approved the final version.

Notes

The authors declare no competing financial interest.

ACKNOWLEDGMENTS

REFERENCES

(1) Hasan, M. Z.; Kane, C. L. Colloquium: topological insulators. *Rev. Mod. Phys.* **2010**, *82*, 3045.

(2) Qi, X.-L.; Zhang, S.-C. Topological insulators and superconductors. *Rev. Mod. Phys.* **2011**, *83*, 1057.

(3) Xu, Y.; et al. Large-gap quantum spin hall insulators in tin films. *Phys. Rev. Lett.* **2013**, *111*, 136804.

(4) Bafekry, A.; et al. Semiconducting chalcogenide alloys based on the (Ge, Sn, Pb)(S, Se, Te) formula with outstanding properties: a first-principles calculation study. *ACS Omega* **2021**, *6*, 9433−9441.

(5) Bafekry, A.; et al. Investigation of vacancy defects and substitutional doping in AlSb monolayer with double layer honeycomb structure: a first-principles calculation. *J. Phys.: Condens. Matter* **2022**, *34*, 065701.

(6) Bafekry, A.; et al. Puckered penta-like PdPX(X= O, S, Te) semiconducting nanosheets: first-principles study of the mechanical, electro-optical, and photocatalytic properties. *ACS Appl. Mater. Interfaces* **2022**, *14*, 21577−21584.

(7) Kane, C. L.; Mele, E. J. Quantum spin hall effect in graphene. *Phys. Rev. Lett.* **2005**, *95*, 226801.

(8) Liu, C.-C.; Jiang, H.; Yao, Y. Low-energy effective hamiltonian involving spin-orbit coupling in silicene and two-dimensional germanium and tin. *Phys. Rev. B* **2011**, *84*, 195430.

(9) Liu, C.-C.; Feng, W.; Yao, Y. Quantum spin hall effect in silicene and two-dimensional germanium. *Phys. Rev. Lett.* **2011**, *107*, 076802.

(10) Houssa, M.; et al. Topological to trivial insulating phase transition in stanene. *Nano Research* **2016**, *9*, 774−778.

(11) Si, C.; et al. Functionalized germanene as a prototype of large-gap two-dimensional topological insulators. *Phys. Rev. B* **2014**, *89*, 115429.

(12) Zhang, H.; Ma, Y.; Chen, Z. Quantum spin hall insulators in strain-modified arsenene. *Nanoscale* **2015**, *7*, 19152−19159.

(13) Zhang, S.; et al. Antimonene oxides: emerging tunable direct bandgap semiconductor and novel topological insulator. *Nano Lett.* **2017**, *17*, 3434−3440.

(14) Ma, Y.; Dai, Y.; Kou, L.; Frauenheim, T.; Heine, T. Robust two-dimensional topological insulators in methyl-functionalized bismuth, antimony, and lead bilayer films. *Nano Lett.* **2015**, *15*, 1083−1089.

(15) Molle, A.; et al. Buckled two-dimensional xene sheets. *Nat. Mater.* **2017**, *16*, 163−169.

(16) Qian, X.; Liu, J.; Fu, L.; Li, J. Quantum spin hall effect in two-dimensional transition metal dichalcogenides. *Science* **2014**, *346*, 1344−1347.

(17) Zhou, S.; Liu, C.-C.; Zhao, J.; Yao, Y. Monolayer group-iii monochalcogenides by oxygen functionalization: a promising class of two-dimensional topological insulators. *npj Quantum Materials* **2018**, *3*, 16.

(18) Weng, H.; et al. Large-gap two-dimensional topological insulator in oxygen functionalized mxene. *Phys. Rev. B* **2015**, *92*, 075436.

(19) Ma, Y.; Kou, L.; Dai, Y.; Heine, T. Proposed two-dimensional topological insulator in site. *Phys. Rev. B* **2016**, *94*, 201104.

(20) Weng, H.; Dai, X.; Fang, Z. Transition-metal pentatelluride ZrTe$_5$ and HfTe$_5$: A paradigm for large-gap quantum spin hall insulators. *Physical Review X* **2014**, *4*, 011002.

(21) Zhou, J.-J.; Feng, W.; Liu, C.-C.; Guan, S.; Yao, Y. Large-gap quantum spin hall insulator in single layer bismuth monobromide bi4br4. *Nano Lett.* **2014**, *14*, 4767−4771.

(22) Bernevig, B. A.; Hughes, T. L.; Zhang, S.-C. Quantum spin hall effect and topological phase transition in hgte quantum wells. *Sscience* **2006**, *314*, 1757−1761.

(23) Wu, S.; et al. Observation of the quantum spin hall effect up to 100 K in a monolayer crystal. *Science* **2018**, *359*, 76−79.

(24) Malyi, O. I.; Dalpian, G. M.; Zhao, X.-G.; Wang, Z.; Zunger, A. Realization of predicted exotic materials: The burden of proof. *Mater. Today* **2020**, *32*, 35−45.

(25) Wu, J.; et al. Controlled chlorine plasma reaction for noninvasive graphene doping. *J. Am. Chem. Soc.* **2011**, *133*, 19668−19671.

(26) Shen, N.; et al. Large gap two-dimensional topological insulators with the coexistence of a significant rashba effect and piezoelectricity in functionalized PbGe monolayers. *Nanoscale* **2023**, *15*, 4045−4052.

(27) Zhang, L.; et al. Two-dimensional honeycomb-kagome Ta$_2$S$_3$: a promising single-spin Dirac fermion and quantum anomalous hall insulator with half-metallic edge states. *Nanoscale* **2019**, *11*, 5666−5673.

(28) Mellaerts, S.; et al. Two dimensional V$_2$O$_3$ and its experimental feasibility as robust room-temperature magnetic Chern insulator. *npj 2D Materials and Applications* **2021**, *5*, 65.

(29) Meng, R.; et al. Hole-doping induced ferromagnetism in 2D materials. *npj Computational Materials* **2022**, *8*, 230.

(30) Zhou, L.; et al. New family of quantum spin hall insulators in two-dimensional transition-metal halide with large nontrivial band gaps. *Nano Lett.* **2015**, *15*, 7867−7872.

(31) Sholl, D. S.; Steckel, J. A. *Density Functional Theory: A Practical Introduction*; John Wiley & Sons, 2022.

(32) Meng, R.; et al. Ferromagnetism and half-metallicity in two-dimensional m o (m= ga, in) monolayers induced by hole doping. *Physical Review Materials* **2020**, *4*, 074001.

(33) Marrazzo, A. Thermal robustness of the quantum spin hall phase in monolayer WTe$_2$. *Physical Review Materials* **2023**, *7*, L021201.

(34) Vergniory, M. G.; et al. All topological bands of all nonmagnetic stoichiometric materials. *Science* **2022**, *376*, No. eabg9094.

(35) Yu, R.; Qi, X. L.; Bernevig, A.; Fang, Z.; Dai, X. Equivalent expression of Z$_2$ topological invariant for band insulators using the non-abelian berry connection. *Phys. Rev. B* **2011**, *84*, 075119.

(36) Li, X.; et al. MoTe$_2$ is a good match for GeI by preserving quantum spin hall phase. *Nano research* **2017**, *10*, 2823−2832.

(37) Kou, L.; et al. Robust 2D topological insulators in van der waals heterostructures. *ACS Nano* **2014**, *8*, 10448−10454.

(38) Björkman, T.; Gulans, A.; Krasheninnikov, A. V.; Nieminen, R. M. van der waals bonding in layered compounds from advanced density-functional first-principles calculations. *Phys. Rev. Lett.* **2012**, *108*, 235502.

(39) Smabraten, D. R.; et al. Electronic structure and surface chemistry of hexagonal boron nitride on HOPG and nickel substrates. *ACS Omega* **2023**, *8*, 24813−24830.

(40) Chen, M.; Weinert, M. Layer *k*-projection and unfolding electronic bands at interfaces. *Phys. Rev. B* **2018**, *98*, 245421.

(41) Kresse, G.; Joubert, D. From ultrasoft pseudopotentials to the projector augmented-wave method. *Phys. Rev. B* **1999**, *59*, 1758.

(42) Kresse, G.; Furthmüller, J. Efficient iterative schemes for *ab initio* total-energy calculations using a plane-wave basis set. *Phys. Rev. B* **1996**, *54*, 11169.

(43) Perdew, J. P.; Burke, K.; Ernzerhof, M. Generalized gradient approximation made simple. *Phys. Rev. Lett.* **1996**, *77*, 3865.

(44) Heyd, J.; Scuseria, G. E.; Ernzerhof, M. Hybrid functionals based on a screened Coulomb potential. *J. Chem. Phys.* **2003**, *118*, 8207−8215.

(45) Grimme, S.; Antony, J.; Ehrlich, S.; Krieg, H. A consistent and accurate ab initio parametrization of density functional dispersion correction (DFT-D) for the 94 elements H-Pu. *J. Chem. Phys.* **2010**, *132*, 154104.

(46) Wang, V.; Xu, N.; Liu, J.-C.; Tang, G.; Geng, W.-T. Vaspkit: A user-friendly interface facilitating high-throughput computing and analysis using vasp code. *Comput. Phys. Commun.* **2021**, *267*, 108033.

(47) Lyakhov, A. O.; Oganov, A. R.; Stokes, H. T.; Zhu, Q. New developments in evolutionary structure prediction algorithm USPEX. *Comput. Phys. Commun.* **2013**, *184*, 1172−1182.

(48) Togo, A.; Tanaka, I. First principles phonon calculations in materials science. *Scripta Materialia* **2015**, *108*, 1−5.

(49) Shuichi, N. Constant temperature molecular dynamics methods. *Prog. Theor. Phys. Suppl.* **1991**, *103*, 1−46.

(50) Nosé, S. A unified formulation of the constant temperature molecular dynamics methods. *J. Chem. Phys.* **1984**, *81*, 511−519.

(51) Mostofi, A. A.; et al. An updated version of wannier90: A tool for obtaining maximally-localised wannier functions. *Comput. Phys. Commun.* **2014**, *185*, 2309−2310.

(52) Wu, Q.; Zhang, S.; Song, H.-F.; Troyer, M.; Soluyanov, A. A. Wanniertools: An open-source software package for novel topological materials. *Comput. Phys. Commun.* **2018**, *224*, 405−416.

(53) Sancho, M. L.; Sancho, J. L.; Sancho, J. L.; Rubio, J. Highly convergent schemes for the calculation of bulk and surface green functions. *Journal of Physics F: Metal Physics* **1985**, *15*, 851.